Available online at www.sciencedirect.com

ScienceDirect

journal homepage: www.elsevier.com/locate/he

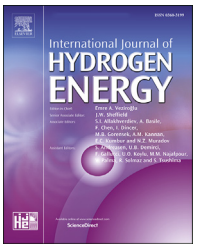

Model construction and energy management system of lithium battery, PV generator, hydrogen production unit and fuel cell in islanded AC microgrid

*Yong Zhang, Wei Wei**

College of Electrical Engineering, Zhejiang University, Hangzhou, 310027, China

HIGHLIGHTS

- Model constructions of different units in AC microgrid.
- Control strategy for SoC and over- power protection.
- *P-f* droop control strategy is designed for PV generator.
- MEP and MPP control strategies are designed for HPU and fuel cell.
- Fuel cell can work from MEP mode to MPP mode to supply the local loads.

ARTICLE INFO

Article history:
Received 18 February 2020
Received in revised form
16 April 2020
Accepted 18 April 2020
Available online xxx

Keywords:
Lithium battery
PV generator
Hydrogen production unit
Fuel cell
Model construction
Energy management system

ABSTRACT

The external electrical characteristics of the lithium battery, PV generator, hydrogen production unit (HPU) and fuel cell in islanded AC microgrid are well analyzed with mathematic models, based on which an energy management system among the abovementioned elements is proposed by using the bus frequency signaling. Specifically, the functions of lithium battery with the variables of the residual capacity and instantaneous working power are well designed to deliver its operation information to other units. The *P-f* droop control strategy is designed for the PV generator to make it adaptively work off from the maximum power point to the reference power point. The control strategy of HPU can make it work from the maximum efficiency point mode to the allowable maximum power point mode to absorb PV output power as much as possible when the lithium battery is almost getting full charged. Similarly, the fuel cell controller can regulate its power generation from the maximum efficiency point mode to the maximum power point to supply the local load as much as possible when the lithium battery is almost getting full discharged. Finally, the proposed energy management system is verified based on RTLAB experimental platform to show the effectiveness of the proposed coordination control strategy.

* *Corresponding author.*
E-mail address: wwei@zju.edu.cn (W. Wei).

https://doi.org/10.1016/j.ijhydene.2020.04.155

Introduction

The distributed renewable energy generation technology has been deeply researched to supply power for the islanders or remote villagers [1–4]. Because renewable energy sources (RES) can be usually obtained inexhaustibly in the local place and exploited without pollution. Besides, the long transmission lines and power towers from the main grid to users are avoided. Especially, the AC microgrid has been widely focused and applied with advantages [5–8]. AC microgrid can be accessed directly to the widely used AC household appliances without changing their habits. Furthermore, AC microgrid is very compatible with the traditional main power grid, and its flexibility and expansibility can improve the power quality and reliability of the power supply.

However, there are also some shortcomings that hinder the promotion of the distributed generation in AC microgrid [9–13]. The fluctuation and intermittence of RESs damage the safe operation of the system, and the power generation characteristics of RESs don't match the load characteristics very much. Furthermore, the access of a large number of RESs will change the traditional power flow direction and challenge the relay protection [9,10]. Therefore, there exists large curtailment or abandoned phenomenon of the RESs in practice [11,12]. Normally, a lithium battery is employed to address the abovementioned disadvantages. It owns the merits of high efficiency, high power density, long lifespan and fast dynamic response, but the expensive price and safety issue should deserve careful consideration [13]. In summary, the lithium battery with an appropriate capacity is generally configured in the microgrid, which can suppress the power fluctuation, absorb the power from RESs in the charging condition and release the power to supply the local load in the discharging condition. But it is very expensive and uneconomical to use a large-capacity lithium battery to absorb the renewable energy power.

The technology of the alkaline electrolysis system for hydrogen production unit (HPU) under the action of platinum catalyst has been focused by many Energy Administrations around the world [3,14–16]. Compared with pumped-storage hydro [17], phase-change material storage [18], flywheel energy storage [19] and superconducting energy storage [20], etc, HPU technology has low requirements for geographical location and environment factors, and the acceptable price and the compact volume can promote its wide application in a modular way. Besides, HPU achieves the long-term and large-capacity power absorption, which can solve the power curtailment problem of RESs. Furthermore, HPU requires not very much for the power quality that can tolerate the shortcomings of RESs. Moreover, the hydrogen energy is widely required in metallurgy, medical treatment, fuel and other industries. Meanwhile, the hydrogen energy can be fed back to the power grid through the fuel cell. Thus, the hydrogen energy becomes the junction of electric energy, chemical energy and thermal energy, which can effectively promote the comprehensive development of ubiquitous Internet of Things.

The well-designed energy management system for microgrid is very significant to promote the coordination operation among the different elements. The state-of-art research methods are investigated as follows. Ref. [21] Proposed a distributed control strategy based on the dc bus signaling for a modular PV generation system. But the dc bus voltage may fluctuate because of the frequent switching among various modes. Ref. [22] Proposed a mode-adaptive decentralized dc microgrid control strategy which owns the merits of seamless mode transition and reliable power sharing. But it is assumed that the state of charge (SoC) of the storage is always in a safe range. In addition, ref. [23] Proposed a double-quadrant SoC-based droop control method for distributed energy storage system to reach the proper power distribution in the autonomous dc microgrids. Ref. [24] Proposed a decentralized control method to realize the generation-storage coordination based on the dc bus voltage signaling. But the dc bus voltage is easily affected by the line resistances in the abovementioned dc microgrid and would degrade the control accuracy of the energy management system. In addition, a very large-capacity storage battery is necessary to suppress the fluctuation of the voltage and consume the surplus RES power. Meanwhile, ref. [25] Presented a control-oriented modeling of an electrolyzer and the auxiliary system for the hydrogen-production process, which can assess the active wind-energy conversion system. Ref. [26] Proposed an optimal stochastic coordinated scheduling method for the distributed RES generation with consideration of the hydrogen storage to consume electric power. Ref. [27] Presented a detailed case to show the potential for producing hydrogen in Brazil by using excess energy from hydroelectric and wind farms. But these literatures didn't talk about the short-term control with consideration of their electrical characteristics. Ref. [28] Proposed a model predictive control technique to coordinate the operation of PV generator, wind turbine and storage battery in the microgrid, but the hydrogen storage wasn't considered in the energy management system. Ref. [29] Designed the decentralized coordination control among the PV/battery/HPU/fuel cell in the islanded AC microgrid, but the external electrical characteristic of the fuel cell was not considered. The summary of the presented methods is concluded in Table 1.

Compared with presented researches in Table 1, the contribution and novelty of this paper are illustrated as follows. This paper proposes a well-designed energy management system for the islanded AC microgrid including the lithium battery, PV generator, HPU and fuel cell with consideration of their respective electrical characteristics. The

Table 1 – Comparison with existing methods.

	A	B	C	d	e	F	g	h
Ref. [21]	✗	✗	✓	✗	✗	✗	✗	✗
Ref. [22]	✗	✗	✗	✗	✓	✗	✗	✗
Ref. [23]	✗	✗	✓	✗	✓	✗	✗	✗
Ref. [24]	✗	✗	✓	✓	✓	✗	✗	✗
Refs. [25–27]	✓	✓	✗	✗	✗	✓	✗	✗
Ref. [28]	✓	✓	✓	✗	✗	✗	✗	✗
Ref. [29]	✓	✓	✓	✓	✓	✓	✓	✗
This paper	✓	✓	✓	✓	✓	✓	✓	✓

a: AC microgrid; b: avoid the influenced by line resistances; c: SoC protection; d: Over power protection; e: Decentralization; f: Large-capacity consumption of electric power; g: Energy conversion efficiency of HPU; h: Electrical characteristic of the fuel cell.

Please cite this article as: Zhang Y, Wei W, Model construction and energy management system of lithium battery, PV generator, hydrogen production unit and fuel cell in islanded AC microgrid, International Journal of Hydrogen Energy, https://doi.org/10.1016/j.ijhydene.2020.04.155

external electrical characteristics of the abovementioned elements are first analyzed in detail according to their mathematic models. Then the overall energy management system and the corresponding control strategy of each element are proposed based on their models. As for the lithium battery, the SoC and the instantaneous working power are considered in the designed functions, which can avoid the battery to be overused or damaged. As for PV generator, the *P-f* droop control is applied to make it work from maximum power point (MPP) mode to the reference power point (RPP) mode seamlessly. As for HPU, the energy conversion efficiency is taken into consideration, and the control strategy can make HPU work from maximum efficiency point (MEP) mode to MPP mode adaptively. As for the fuel cell, there also exists an MPP in the output power curve, thus the control strategy will regulate the power generation from MEP mode to the allowable MPP mode to help the battery supply the local loads. Finally, the proposed control strategy in the energy management system is verified based on the RTLAB experimental platform in various situations.

Model constructions and analysis

Model of the lithium battery

When $LiFePO_4$ battery is in charging process, Li^+ in the positive electrode migrates toward the negative electrode through the polymer membrane. When in discharging process, Li^+ moves in the reverse direction. The chemical equation in the charging or discharging process is explained as

$$\begin{cases} Positive: LiFePO_4 \underset{\text{discharg}}{\overset{\text{charge}}{\rightleftharpoons}} Li_{(1-x)}FeO_4 + xLi^+ + xe^- \\ Negative: 6C + xLi^+ + xe^- \underset{\text{discharge}}{\overset{\text{charge}}{\rightleftharpoons}} Li_x C_6 \end{cases} \quad (1)$$

The lithium battery generally owns the robust external electrical characteristic, which can be similarly regarded as an ideal voltage source. But the equivalent resistance and capacitance are influenced by the remaining capacity of battery. Therefore, the SoC of the lithium battery should be considered in the control strategy. The equivalent circuit of lithium battery is shown in Fig. 1, and the external electrical model is [30,31].

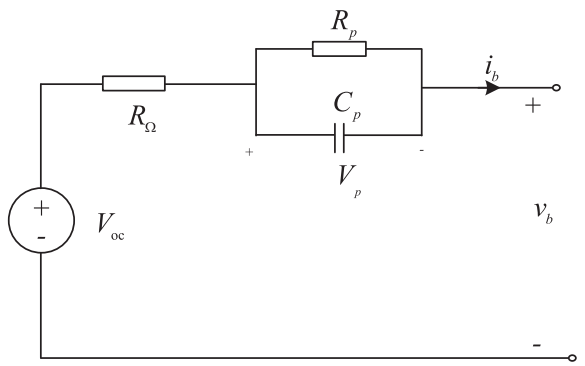

Fig. 1 – Equivalent circuit of lithium battery.

$$v_b(t) = V_{ocv} - V_{C_p}(t) - R_\Omega\, i_b(t), where\ V_{C_p}(t) = \begin{cases} R_p\, i_b(t)\left[1 - e^{\frac{t-t_0}{R_p C_p}}\right], & t_0 < t < t_1 \\ V_{C_p}(t_1) e^{\frac{t-t_1}{R_p C_p}}, & t_1 < t < t_2 \end{cases} \quad (2)$$

where $v_b(t)$ is the terminal voltage, $i_b(t)$ is the working current, R_Ω is the series resistance, R_p is the parallel resistance, C_p is the parallel capacitor, V_{oc} is the open circuit voltage. The battery discharges during $t_0<t<t_1$, and the rest in $t_1<t<t_2$.

Model of PV generator

Photovoltaic (PV) generation technologies have been studied for deeply and the PV scale has been developed rapidly in recent decades of years. The global PV installed capacity increased more than 100 GW year-on-year in 2019, and it continues to maintain this growth rate in the future. The external electrical characteristics of the PV system can be expressed as [32,33].

$$P_{pv} = v_{pv}\, i_{pv} \quad (3)$$

$$i_{pv} = \frac{G}{1000}\left[I_{sc} N_p + 0.0038 N_p (T-25)\right] - \frac{\left[I_{sc} N_p + 0.0038 N_p (T-25)\right]}{\exp(V_{oc}\, q/aNkT) - 1}\left[\exp\left(\frac{v_{pv} + 0.221 i_{pv} N_s/N_p}{N_s\, aNkT/q}\right) - 1\right] \quad (4)$$

where P_{pv} is the total PV output power, i_{pv} is the total working current, v_{pv} is the total terminal voltage, I_{sc} is the short-circuit current of each PV panel, V_{oc} is the open-circuit voltage of each PV panel, N_p is the parallel number of the PV panel, N_s is the series number of PV panel, G is the irradiance intensity, T is the working temperature, q is the electronic charge, k is the Boltzmann's constant, N is the number of PV cell in each PV panel, a is the ideal parameter of the diode.

According to Eqs (3) and (4) as well as the parameters in Table 2, the influences of the working temperature and irradiance intensity on the external electrical characteristics of PV generator are shown in Fig. 2. From Fig. 2(a) and (b), the low temperature contributes to the PV power generation, but the overall influence of the working temperature on the electrical characteristics is very limited. It is because the ambient temperature will not change much in a short time. Besides, the wind can take away the working heat of the outdoor PV panels.

By contrast, it can be found from Fig. 2(c) and (d) that the stronger irradiance can produce larger short-circuit current and output power. Because parts of PV panels are in series

Table 2 – Parameters of the model of PV generator.

Component	Value	Component	Value
I_{sc}	8.21 A	V_{oc}	32.9 V
N_p	27	N_s	10
N	54	A	1.4284
Q	1.6e−19 eV s	K	1.38e-23 J/K

Please cite this article as: Zhang Y, Wei W, Model construction and energy management system of lithium battery, PV generator, hydrogen production unit and fuel cell in islanded AC microgrid, International Journal of Hydrogen Energy, https://doi.org/10.1016/j.ijhydene.2020.04.155

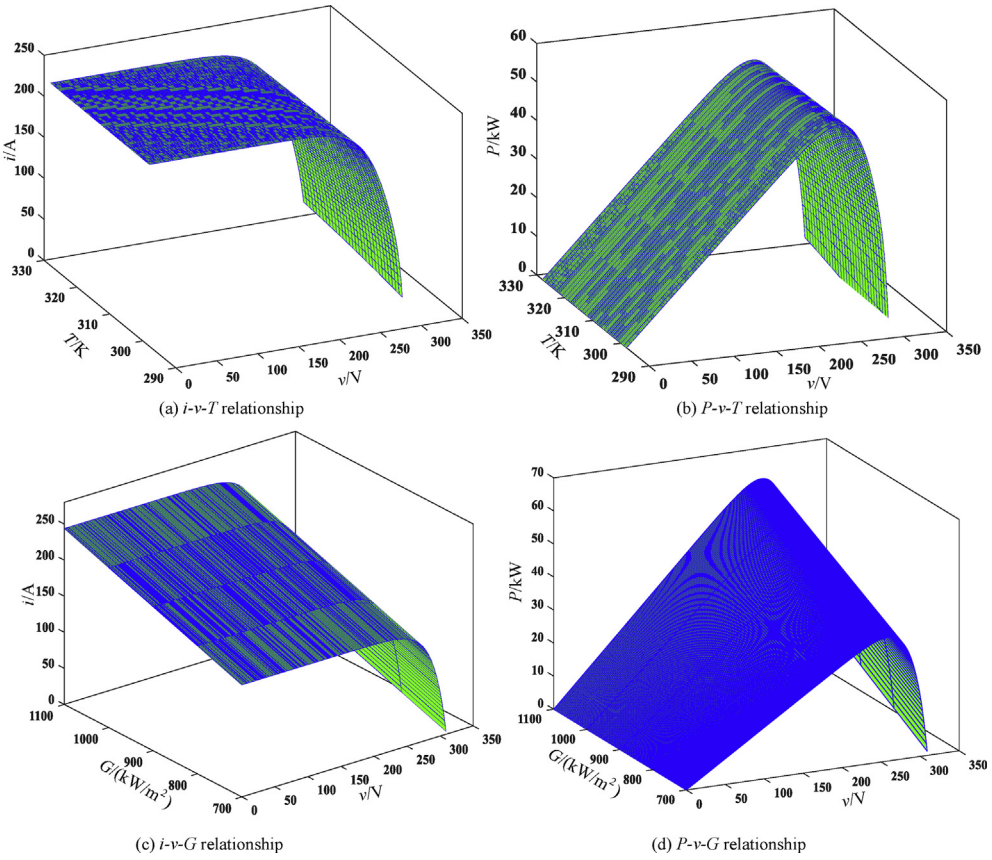

(a) *i-v-T* relationship (b) *P-v-T* relationship

(c) *i-v-G* relationship (d) *P-v-G* relationship

Fig. 2 – Influence of the temperature and irradiance on the electrical characteristics of PV generator.

connection, the shadow not only reduces the working current of the individual PV panel but also degrades the whole PV power generation of the series group. Therefore, the PV panels should be installed on the roof or outdoor so that they can avoid to be shaded by trees or buildings. Furthermore, PV panels should be installed in places with sufficient sunshine throughout the year, and the sufficient clearance is reserved between PV panels to avoid the shadow from the interlaced PV units.

Model of HPU

The chemical reaction principle is explained as that the pure water (H_2O) is electrolyzed to produce chemical hydrogen ions (H^+) and hydroxyl ions (OH^-) under the platinum catalyst. The H^+ in the cathode can combine with electrons (e^-) to produce hydrogen, and the OH^- in the anode produces oxygen by oxidation, which is expressed as

$$\begin{cases} Cathode: \ 4H_2O + 4e^- = 2H_2 \uparrow + 4OH^- \\ Anode: \ 4OH^- - 4e^- = 2H_2O + O_2 \uparrow \end{cases} \tag{5}$$

HPU achieves large-capacity and long-term absorption of electric energy, which can solve the abandonment of renewable power generations. Besides, HPU requires not much power quality of RESs and is becoming a potential energy hub to develop many industries. The external electrical characteristics of HPU are expressed as [34,35].

$$P_h = v_h \, i_h \tag{6}$$

$$v_h = N\left(1.253 - 2.4516e^{-5}\,T + \left(r_1 + \frac{r_2\,T}{A_{ele}}\right)i_h + (s_1 + s_2T + s_3T^2)\log\left[\left(t_1 + \frac{t_2}{T} + \frac{t_3}{T^2} + \frac{\alpha}{A_{ele}}\right)i_h + 1\right]\right) \tag{7}$$

$$\eta\% = \frac{KR_h(1 - \beta T)}{2FV_{rev} + 2F(1-\lambda)\left[\frac{r_1 + r_2T}{A_{ele}}\,i_h + (s_1 + s_2T + s_3T^2)\log\left(\frac{t_1 + \frac{t_2}{T} + \frac{t_3}{T^2} + \alpha}{A_{ele}}i_h + 1\right)\right] + \frac{2FTS}{Ni_h}} \times 100\% \tag{8}$$

Please cite this article as: Zhang Y, Wei W, Model construction and energy management system of lithium battery, PV generator, hydrogen production unit and fuel cell in islanded AC microgrid, International Journal of Hydrogen Energy, https://doi.org/10.1016/j.ijhydene.2020.04.155

Table 3 – Parameters of the model of HPU.

Component	Value	Component	Value	Component	Value
r_1	2.3e-3	t_2	−1.3029e-2	A_{ele}	0.25 m^2
r_2	−1.107e-7	t_3	2.513e-3	N	100
s_1	1.286e-1	A	3	β	2.98e-3
s_2	2.378e-3	F	96,485 C mol^{-1}	R_h	284.7 kJ mol^{-1}
s_3	−0.606e-5	Σ	2	S	90 J $mol^{-1}K^{-1}$
t_1	3.559	K	1300	λ	0.3

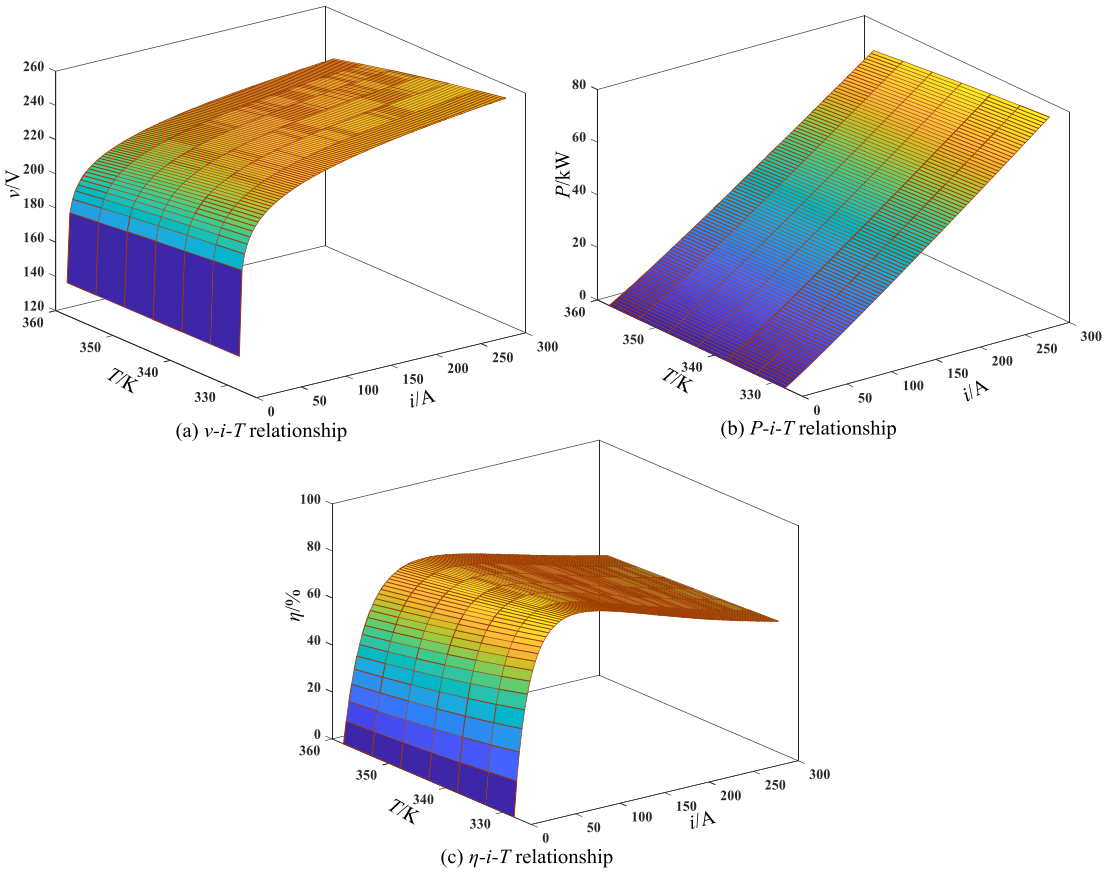

Fig. 3 – Analysis results of hydrogen production unit.

The variables are explained as follows. P_h is the absorbed power. υ_h is the terminal voltage. i_h is the working current. N is the number of the electrolyzer. T is the working temperature. A_{ele} is the cathode plate area. K is electrochemical equivalent coefficient. F is the Faraday coefficient. R_h is the calorific value coefficient of hydrogen. S is the entropy value. λ is the thermal dissipation coefficient. r_1, r_2, s_1, s_2, s_3, t_1, t_2, t_3, α, and β are the correlation coefficients.

Based on the above equations and the parameters in Table 3, the intuitive diagrams are drawn as Fig. 3 to clearly show their relationship. Fig. 3(a) shows the relationship among the terminal voltage, working current and the working temperature. It can be found that the terminal voltage increases rapidly with the increase of the working current at first because of the reversible voltage formed in the chemical reaction. Then the terminal voltage increases slowly with the working current. The high temperature will degrade the terminal voltage and reduce the power absorption. But the power consumption will increase with the working current and the working temperature on the whole as shown in Fig. 3(b).

The energy conversion efficiency from electric energy to chemical energy is drawn in Fig. 3(c). The energy conversion efficiency increases first and then decreases slowly with the increase of the working current. It is because the auxiliary equipments such as pumps and solenoids consume part of the electric energy, and the energy conversion efficiency will increase with the power consumption of HPU. However, the high working current also causes the serious ohmic polarization and concentration polarization phenomenon, which will produce the energy loss, suppress the chemical reaction, and degrade the energy conversion efficiency.

Please cite this article as: Zhang Y, Wei W, Model construction and energy management system of lithium battery, PV generator, hydrogen production unit and fuel cell in islanded AC microgrid, International Journal of Hydrogen Energy, https://doi.org/10.1016/j.ijhydene.2020.04.155

Model of the fuel cell

Hydrogen gas (H_2) can be converted into hydrogen ions (H^+) with the catalyst and the H^+ will diffuse to the cathode plate and produce water (H_2O) with the oxygen (O_2) in the air. The principle of the fuel cell is shown as

$$\begin{cases} Anode: \ 2H_2 - 4e^- = 4H^+ \\ Cathode: \ O_2 + 4H^+ + 4e^- = 2H_2O \end{cases} \tag{9}$$

The fuel cell can support the key load when SoC of lithium battery is very low at night. In addition, the large-capacity storage of hydrogen gas will cause leakage and safety issues, hence the fuel cell is necessary to consume the hydrogen gas and feedback power to the microgrid. The external characteristics of the fuel cell is written as [36,37].

$$P_{fc} = v_{fc}\, i_{fc} \tag{10}$$

$$v_{fc} = n\left[\begin{array}{l} 1.299 - 8.5\times10^{-4}(T-298.15) - 4.308\times10^{-5}\,T(\ln P_{H_2} + 0.5\ln P_{O_2}) - \delta_1 - \\ \left(\delta_2 + 2\times10^{-4}\ln A + 4.5\times10^{-5}\ln\left(P_{H_2}\times 9.17\times10^{-7}\times e^{-\frac{77}{T}}\right)\right)T - \delta_3\, T\ln\left(P_{O_2}\times 1.97\times10^{-7}\times e^{\frac{498}{T}}\right) \\ -\delta_4\, T\ln i_{fc} - \left(R_t + \dfrac{181.6\left[1+0.03\dfrac{i_{fc}}{A}+0.06\left(\dfrac{T}{303}\right)^2\left(\dfrac{i_{fc}}{A}\right)^{2.5}\right]l}{\left[\sigma - 0.634 - 3\left(\dfrac{i_{fc}}{A}\right)\exp\left(4.18\dfrac{T-303}{T}\right)\right]A}\right)i_{fv} - m_1\exp\left(-\dfrac{m_2 i_{fc}}{A}\right) \end{array}\right] \tag{11}$$

$$\eta_{\max} = \frac{v_{fc}}{S_{H_2}L} \tag{12}$$

The variables are explained as follows. P_{fc} is the power generation. v_{fc} is the terminal voltage. i_{fc} is the working current. N is the number of the fuel cell. A is the cross-section area of the membrane interface. P_{H2} and P_{O2} are the pressure values of hydrogen and oxygen flowing into the fuel cell. L is the equal voltage of lower heating value of hydrogen. S_{H2} is the hydrogen stoichiometry. δ_1, δ_2, δ_3, δ_4, m_1, m_2, σ, R_t are the empirical coefficients.

Based on above equations and parameters in Table 4, the relationships among the voltage, current, temperature and power are drawn as Fig. 4. From Fig. 4(a), the terminal voltage decreases with the increase of working current on the whole. Because the large working current causes ohmic polarization and concentration polarization, which will degrade the terminal voltage. The high working temperature can contribute to a large terminal voltage a little, but it is very limited. From Fig. 4(b), the working current has much more influence than the temperature on the power generation, and there exists a peak power point in each curve.

Energy management system of the islanded AC microgrid

The bus frequency f_{bus} of the AC microgrid is supported by the controller of the lithium battery. There are three kinds of key cases in the energy management system as shown in Fig. 5.

(i) The battery is overcharged in the sunny day. When the PV output power is much more than the power consumption of the local load and HPU, the surplus power will flow into the lithium battery. When the SoC and instantaneous power of the battery are in the safe range, f_{bus} will remain at the rated value f_n. If the SoC or instantaneous charging power exceeds the setting value, f_{bus} will increase correspondingly. When f_{bus} is increased from f_n to f_1, HPU will perceive the change of frequency and adjust its working condition from MEP mode to MPP mode to absorb much more power. Meanwhile, PV generator still works at the MPP to generate power as much as possible. When f_{bus} increases from f_1 to f_2, it means that HPU cannot consume the extra PV power even though it operates at the allowable MPP. Then PV generator will adaptively work off from the MPP to suppress the continuous increasement of the bus frequency. Finally, the battery is floating charged and PV generator supplies the local load and HPU.

(ii) The battery is over discharged in the cloudy or thunderstorm day. The PV output power is very limited because the irradiance is relatively weak in the cloudy

Table 4 – Parameters of the model of fuel cell.

Component	Value	Component	Value	Component	Value
δ_1	−0.4185	Σ	15.9	A	50 cm^2
δ_3	0.0135	R_t	4e-5	N	70
δ_2	0.2	m_1	0.2083	S_{H2}	1.15
δ_4	-4e-5	m_2	50.73	L	1.25

Please cite this article as: Zhang Y, Wei W, Model construction and energy management system of lithium battery, PV generator, hydrogen production unit and fuel cell in islanded AC microgrid, International Journal of Hydrogen Energy, https://doi.org/10.1016/j.ijhydene.2020.04.155

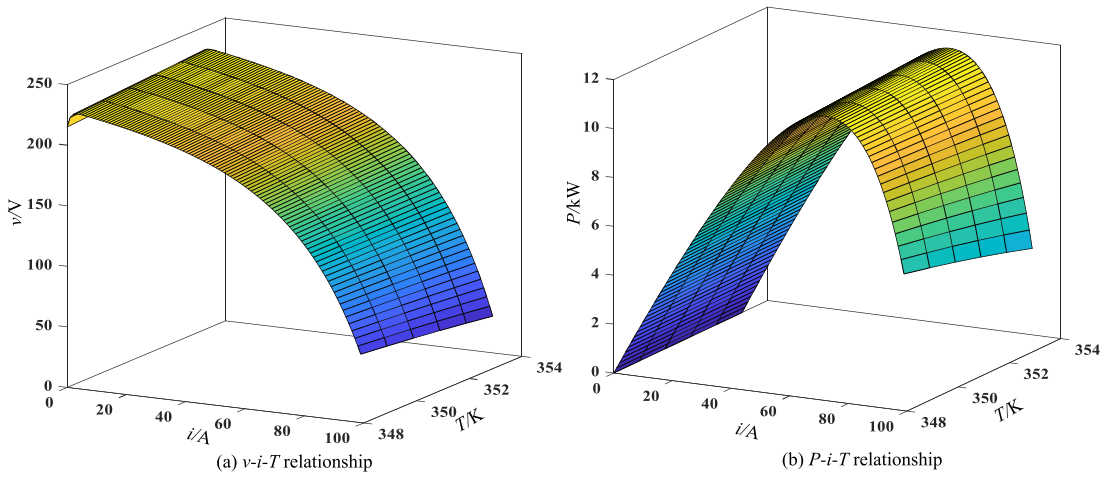

Fig. 4 – Analysis results of fuel cell.

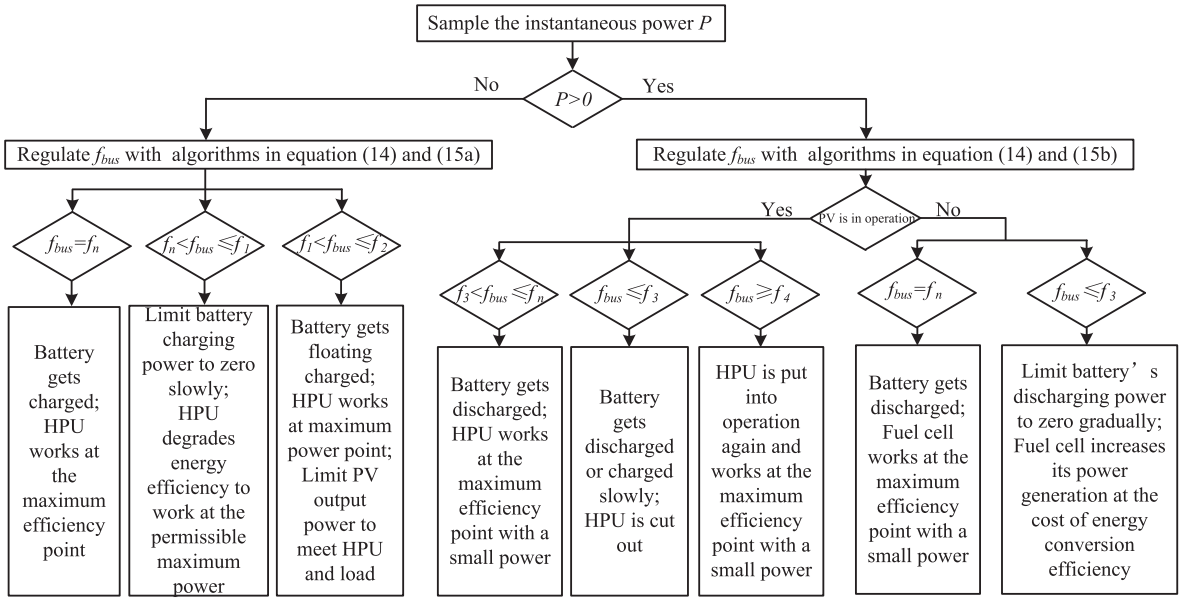

Fig. 5 – Flow chart of the energy management system.

day. The battery needs to discharge to help supply the local load and HPU. If the SoC or instantaneous discharging power exceeds the setting value, f_{bus} will decrease correspondingly. When f_{bus} is decreased from f_n to f_3, HPU will detect the bus frequency and stop working. Then PV generator will supply the local load and the extra power flows into the battery. Once the irradiance is getting restored, the large surplus PV output power will continue to charge the battery and make the SoC increase rapidly. If f_{bus} restores to the setting value f_4, HPU will operate again.

(iii) The battery is over discharged at night. PV generator stops working in the evening, and the battery and fuel cell supply the local load. It should be pointed out that the fuel cell shouldn't be worked with the PV generator and HPU at the same time because of the low energy conversion efficiency from power to gas and then to power at the same time. The fuel cell helps battery supply the important load until the next day. Therefore, when SoC and instantaneous discharging power of the battery are in the safe range, f_{bus} will work at the rated value and the fuel cell will work at MEP mode with a relatively small power generation. When SoC decreases under the safe range, f_{bus} decreases from f_n to f_3. The fuel cell will adaptively regulate its working point from MEP to the allowable MPP seamlessly. Finally, the fuel cell will supply the key loads until the next day. The SoC stops decreasing, and f_{bus} remains unchanged.

Control strategy of the lithium battery

The lithium battery plays as an essential role to support the bus voltage and balance the instantaneous power in the

Please cite this article as: Zhang Y, Wei W, Model construction and energy management system of lithium battery, PV generator, hydrogen production unit and fuel cell in islanded AC microgrid, International Journal of Hydrogen Energy, https://doi.org/10.1016/j.ijhydene.2020.04.155

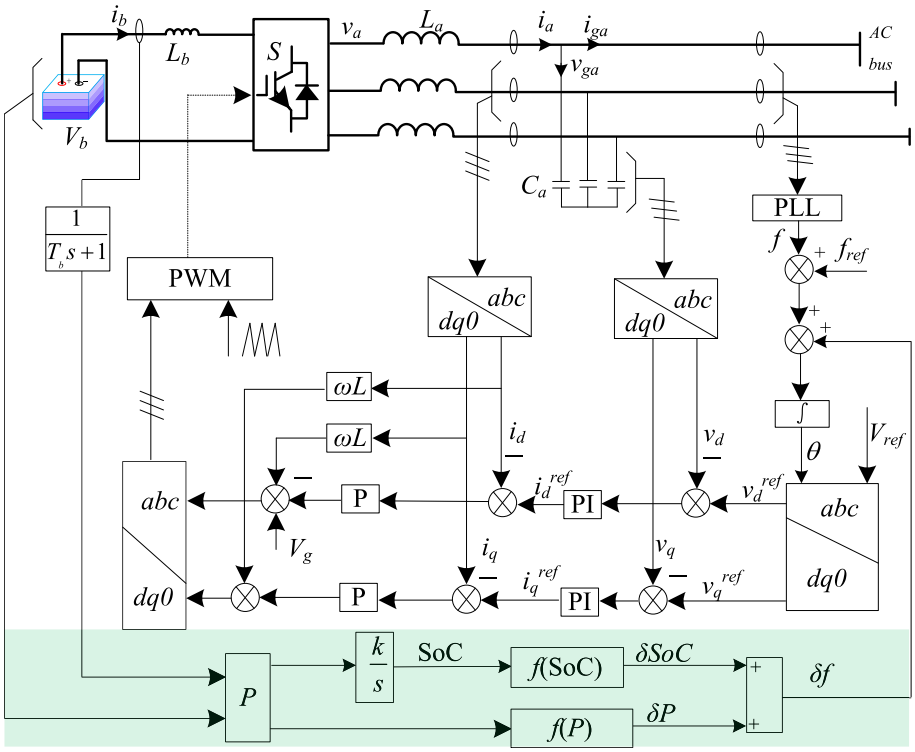

Fig. 6 – Control strategy of the lithium battery.

islanded AC microgrid. A small capacity of battery is configured to save the cost and rich the working conditions here. The control strategy is shown in Fig. 6. The f_{bus} and voltage magnitude are controlled at the rated values in this controller. There are two functions of the SoC and instantaneous power respectively, which are designed to superimpose the results into the frequency reference value. Therefore, the information of the SoC and instantaneous charging or discharging power of the battery can be delivered to other elements in this way. The SoC of the battery is

$$SoC = SoC_{t=0} - \frac{1}{C_b}\int P dt \tag{13}$$

where $SoC_{t=0}$, C_b, P are the SoC at $t = 0$, power capacity and input power respectively.

When the SoC is between SoC_l and SoC_u, the output result of the function is zero. The battery can continue to charge or discharge in this condition, and f_{bus} remains at the rated value. When SoC exceeds the setting value, the well-designed function will transmit this information to other units. The function with the variable of SoC is expressed as

$$f(SoC) = \begin{cases} k_{soc}\,(SoC - SoC_u); & if\ SoC > SoC_u \\ 0; & if\ SoC_l < SoC < SoC_u \\ k_{soc}\,(SoC - SoC_l); & if\ SoC < SoC_l \end{cases} \tag{14}$$

where k_{soc} is the designed coefficient, SoC_u and SoC_l are the upper and lower setting values.

The large instantaneous charging or discharging power would damage the inverter even though the SoC is in the safe range. It is defined that the charging power is negative and the discharging power is positive. When the charging power P_{ch} is larger than the negative reference value $-P^*$, the output result is zero. It means the charging power magnitude is in the safe range. When P_{ch} is smaller than $-P^*$, the output result will be linear with the charging power and cause the increasement of the bus frequency. It is similar in the discharging condition. In summary, the function with the variable of instantaneous power is designed as

$$f(P_{ch}) = \begin{cases} 0;\ if\ P_{ch} > -P^* \\ k_p(-P_{ch} - P^*);\ if\ P_{ch} \le -P^* \end{cases} \tag{15a}$$

$$f(P_{disch}) = \begin{cases} 0;\ if\ P_{disch} < P^* \\ k_p(P^* - P_{disch});\ if\ P_{disch}\ ^3\ P^* \end{cases} \tag{15b}$$

where k_p is the designed coefficient, P_{ch} and P_{disch} are the charging and discharging powers respectively, P^* is the allowable maximum power value.

It should be noticed that the charging power would be very large in a low SoC condition when the PV generator starts to work in the morning. In addition, the discharging power would be also very large in a high SoC condition when PV generator stops working in the evening. The large instantaneous working power would damage the inverter and shorten its lifespan. Therefore,Eq. (15) can deliver the information of the instantaneous power to other elements so that HPU and

Please cite this article as: Zhang Y, Wei W, Model construction and energy management system of lithium battery, PV generator, hydrogen production unit and fuel cell in islanded AC microgrid, International Journal of Hydrogen Energy, https://doi.org/10.1016/j.ijhydene.2020.04.155

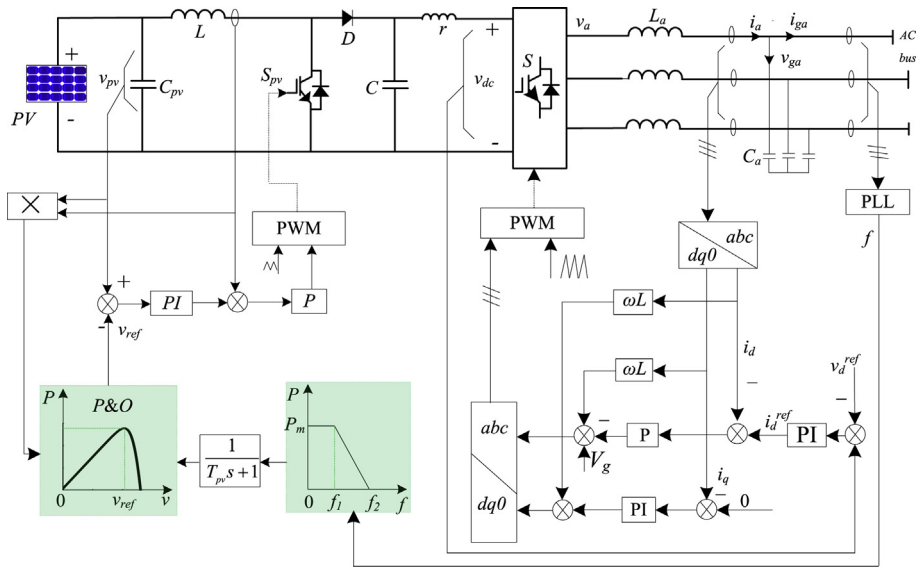

Fig. 7 – Control strategy of PV generator.

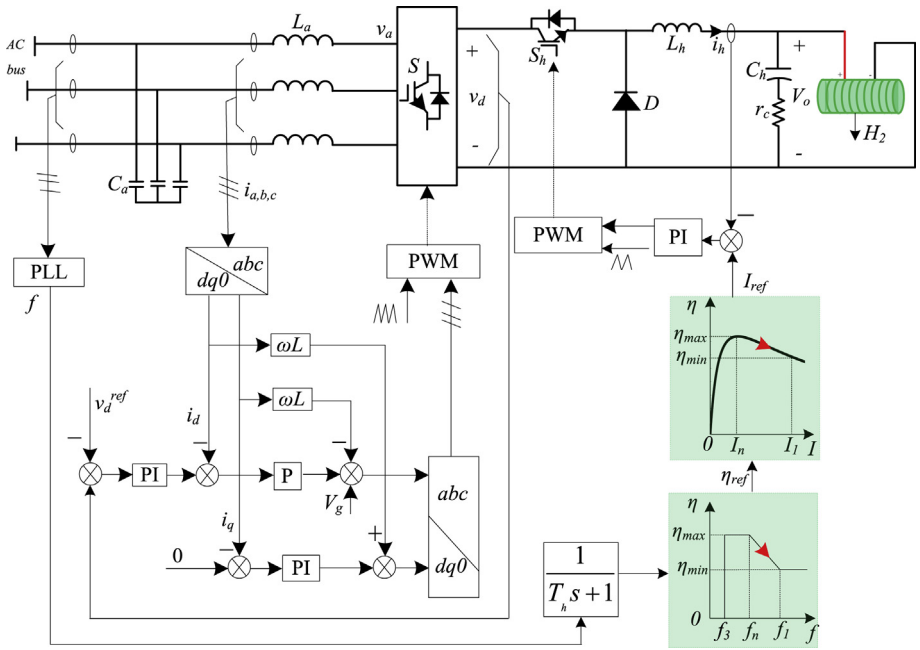

Fig. 8 – Control strategy of HPU.

PV generator can response to avoid the overcharging and over discharging issues.

Control strategy of PV generator

PV generator is connected to the AC bus through a two-stage inverter as shown in Fig. 7. The first stage is used to achieve the maximum power point tracking (MPPT) algorithm. The second stage is used to finish the inverting process and power transmission. When f_{bus} is below the setting value f_1, the output result is P_m. It means the AC microgrid system can consume the maximum power generation of PV generator. When f_{bus} increases from f_1 to f_2, it means the PV output power is more than the power consumption of the local load, HPU and battery in the system. Then the PV generator needs to decrease its power generation with the increase of the bus frequency. The *P-f* droop control strategy is designed as

$$\begin{cases} P_{ref} = P_m - k_{pv}\left(f_{bus} - f_1\right) \\ k_{pv} = \dfrac{P_m}{f_2 - f_1} \end{cases} \tag{16}$$

where k_{pv} is the decreasing slope of the reference power, P_m is

Please cite this article as: Zhang Y, Wei W, Model construction and energy management system of lithium battery, PV generator, hydrogen production unit and fuel cell in islanded AC microgrid, International Journal of Hydrogen Energy, https://doi.org/10.1016/j.ijhydene.2020.04.155

the maximum output power of the PV generator, f_2 is the allowable maximum bus frequency.

The designed control strategy of PV generator can not only guarantee the maximum power generation, but also ensure the stability and reliability of the energy management system. Since the balance of the power flow is preferred to be focused in this paper, MPPT can be achieved by using the traditional perturbation and observation (P&O) algorithm and it is not discussed here.

Control strategy of HPU

HPU can convert the electric energy into the clean hydrogen energy, but the energy conversion efficiency is very important. From the analysis in Section Model of HPU, the power absorption of HPU increases with the increase of the input current, but the energy conversion efficiency increases first and then decreases with the increase of the input current. The control strategy of HPU with consideration of MEP and MPP is shown in Fig. 8.

When f_{bus} remains at the rated value f_n, HPU works at the maximum efficiency value $\eta_{\max}$ with a relative small power consumption. It means the SoC of the battery is in a relatively low condition, and the surplus PV output power can be absorbed by the battery totally. When f_{bus} increases from f_n to f_1, the SoC of the battery is in a relatively high condition, and HPU needs to increase its power consumption to balance the floating power. Finally, HPU will operate at the allowable MPP in this situation at the cost of some energy conversion efficiency. The output result is demonstrated as

$$\begin{cases} \eta_{ref} = \eta_{\max} - k_h \times (f_{bus} - f)_n \\ k_h = \dfrac{\eta_{\max} - \eta_{\min}}{f_1 - f_n} \end{cases} \tag{17}$$

where k_h is the decreasing slope, $\eta_{\max}$ and $\eta_{\min}$ are the allowable maximum and minimum efficiency values.

In addition, when f_{bus} decreases to the setting value f_3, the output result is zero. It means that the SoC of the battery is in a relatively low condition because of the continuous discharging process, and HPU needs to be cut out to ensure the supply of the important local loads.

Control strategy of the fuel cell

It is normally economic to configure a small-capacity battery with a fuel cell in the AC microgrid system. In addition, the produced hydrogen gas needs to be used by the fuel cell, which works as the back-up power to help the battery supply the key load at night. According to the analysis in Section Model of the fuel cell, the power generation of the fuel cell increases first and then decreases with the increase of the input current, hence the MPP needs to be considered in the control strategy. Besides, the MEP usually locating at the left part of MPP should be also taken into consideration. The control strategy of the fuel cell is shown in Fig. 9. When f_{bus} remains at f_n, the output power reference is P_{mep}. It means that the SoC of battery is relatively enough, and the fuel cell works at MEP to help supply the local load. When the bus frequency decreases from f_n to f_3, the output power reference is shown as

$$\begin{cases} P_{ref} = P_{mep} + k_{fc}(f_n - f_{bus}) \\ k_{fc} = \dfrac{P_{mpp} - P_{mep}}{f_n - f_3} \end{cases} \tag{18}$$

where k_{fc} is the increasing slope of the reference power, P_{mep} is the power generation at MEP, P_{mpp} is the power generation at MPP, f_3 is the allowable minimum bus frequency.

From Eq. (18), the reference power value of the fuel cell will increase from P_{mep} to P_{mpp} with the decrease of bus frequency from f_n to f_3. Finally, the fuel cell will help battery supply the key load until the next day. It should be pointed out that the large-capacity fuel cell can help supply much more loads, but a relatively small capacity of the fuel cell is designed here to

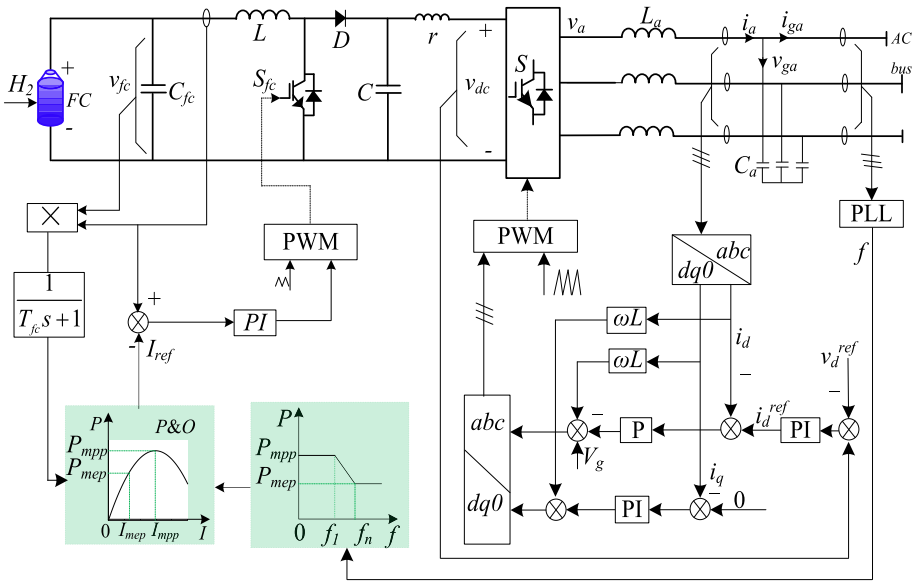

Fig. 9 – Control strategy of the fuel cell.

Please cite this article as: Zhang Y, Wei W, Model construction and energy management system of lithium battery, PV generator, hydrogen production unit and fuel cell in islanded AC microgrid, International Journal of Hydrogen Energy, https://doi.org/10.1016/j.ijhydene.2020.04.155

Table 5 – Parameters of the AC microgrid system.

	Component	Value	Component	Value	Component	Value
Lithium battery	V_{in}	800 V	L	1 mH	C	2000 μF
	V_{dref}	311 V	SoC_u	80%	SoC_u	30%
	f_n	50 Hz	f_1	50.4 Hz	f_2	50.5 Hz
	f_3	49.5 Hz	f_4	49.9 Hz	T_b	0.001
	k_{soc}	0.3	k_p	1e-6	k_{vp_d}	0.8
	k_{vi_d}	100	k_{ip_d}	1	k_{vp_q}	0.8
	k_{vi_q}	100	k_{ip_q}	1		
PV generator	C_{pv}	500 μF	L_{dc}	2 mH	C_{dc}	1000 μF
	k_{vp}	5	k_{vi}	200	k_{ip}	0.001
	L	2000 mH	C	2000 μF	V_{dref}	600 V
	k_{pv}	2e4	T_{pv}	0.001	k_{vp_d}	1
	k_{vi_d}	10	k_{ip_d}	1	k_{ip_q}	10
	k_{ii_q}	100				
HPU	L_{dc}	4 mH	C_{dc}	2000 μF	k_{ip}	1
	k_{ii}	200				
	L	1 mH	C	1000 μF	k_{vp_d}	1
	k_{vi_d}	10	k_{ip_d}	1	k_{ip_q}	10
	k_{ii_q}	100	k_h	4		
Fuel cell	L_{dc}	4 mH	C_{dc}	2000 μF	k_{ip}	1
	k_{ii}	200				
	L	1 mH	C	1000 μF	k_{vp_d}	1
	k_{vi_d}	10	k_{ip_d}	1	k_{ip_q}	10
	k_{ii_q}	100	k_{fc}	1.8e4		

rich the working conditions. Therefore, some unimportant loads should be cut out at the same time.

In summary, the control strategies of the lithium battery, PV generator, HPU and fuel cell are designed with consideration of their electrical characteristics respectively in this section. The SoC and instantaneous power of the battery are considered in the control strategy to guarantee the safe operation. The *P-f* droop control of PV generator is designed to make it work off from MPP to RPP adaptively. The energy conversion efficiency of HPU is considered in the control strategy. When the PV output power is relatively limited, HPU will work at MEP with a small power consumption. When the PV power generation is very large, HPU will adaptively regulate the power absorption from MEP to the allowable MPP. As for the fuel cell, when the SoC of battery is very enough, the fuel cell will work at MEP to guarantee the high energy conversion efficiency. When the SoC of battery is very low, the fuel cell will work from MEP to the MPP adaptively to help the battery supply the local load until the next day.

Control results

RTLAB is an industrial real-time platform which can calculate the high dynamic and real-time model, especially for the complex problems that require high fidelity response and high accuracy. The AC microgrid system containing the lithium battery, PV generator, HPU, fuel cell and local loads is built in RTLAB version 11.2.2.108 experimental platform based on the parameters in Table 5. The results are presented as follows to verify the energy management system applied in the islanded AC microgrid in various kinds of situations.

Control results in the sunny day

The control results in the sunny day situation are shown in Fig. 10. Fig. 10(a) shows the waveform of the bus frequency f_{bus}. Fig. 10(b) shows the waveforms of the PV output power P_{PV} and the three-phase inductive current i_{LPV}. Fig. 10(c) shows key waveforms of HPU including the energy conversion efficiency η%, power absorption P_{HPU}, and the three-phase inductive current i_{LHPU}. Fig. 10(d) shows the local load waveform. Fig. 10(e) shows the waveforms of the battery containing the SoC, instantaneous charging power P_b, three-phase inductive current i_{Lb}, the function results δSoC and δP. The waveforms are divided into four stages.

During stage I, the SoC increases from 72% to about 80%, and the bus frequency almost keeps at 50 Hz. The PV generator works at the MPP mode and the output power is about 45 kW in the morning. The local load is about 20 kW. HPU works at the MEP point. The energy conversion efficiency is about 70% and the power consumption is about 20 kW. The surplus 5 kW will flow into the battery. Because the SoC and the charging power are in the safe range, the function result δP of Eq. (15) is zero. In addition, the bus frequency fluctuates a little. But it needs a transition process for other elements to perceive and response to this variation. In fact, the stage I appears most of the time in practice, but a small-capacity battery is configured here to rich the working conditions.

During stage II, the PV output power increases rapidly because the irradiance density increases from 600 kW/m^2 to 1000 kW/m^2. The SoC of the battery increases immediately because the surplus PV power flows into the battery, which will cause the increasement of the bus frequency. HPU perceives the variation of the bus frequency and adaptively works

Please cite this article as: Zhang Y, Wei W, Model construction and energy management system of lithium battery, PV generator, hydrogen production unit and fuel cell in islanded AC microgrid, International Journal of Hydrogen Energy, https://doi.org/10.1016/j.ijhydene.2020.04.155

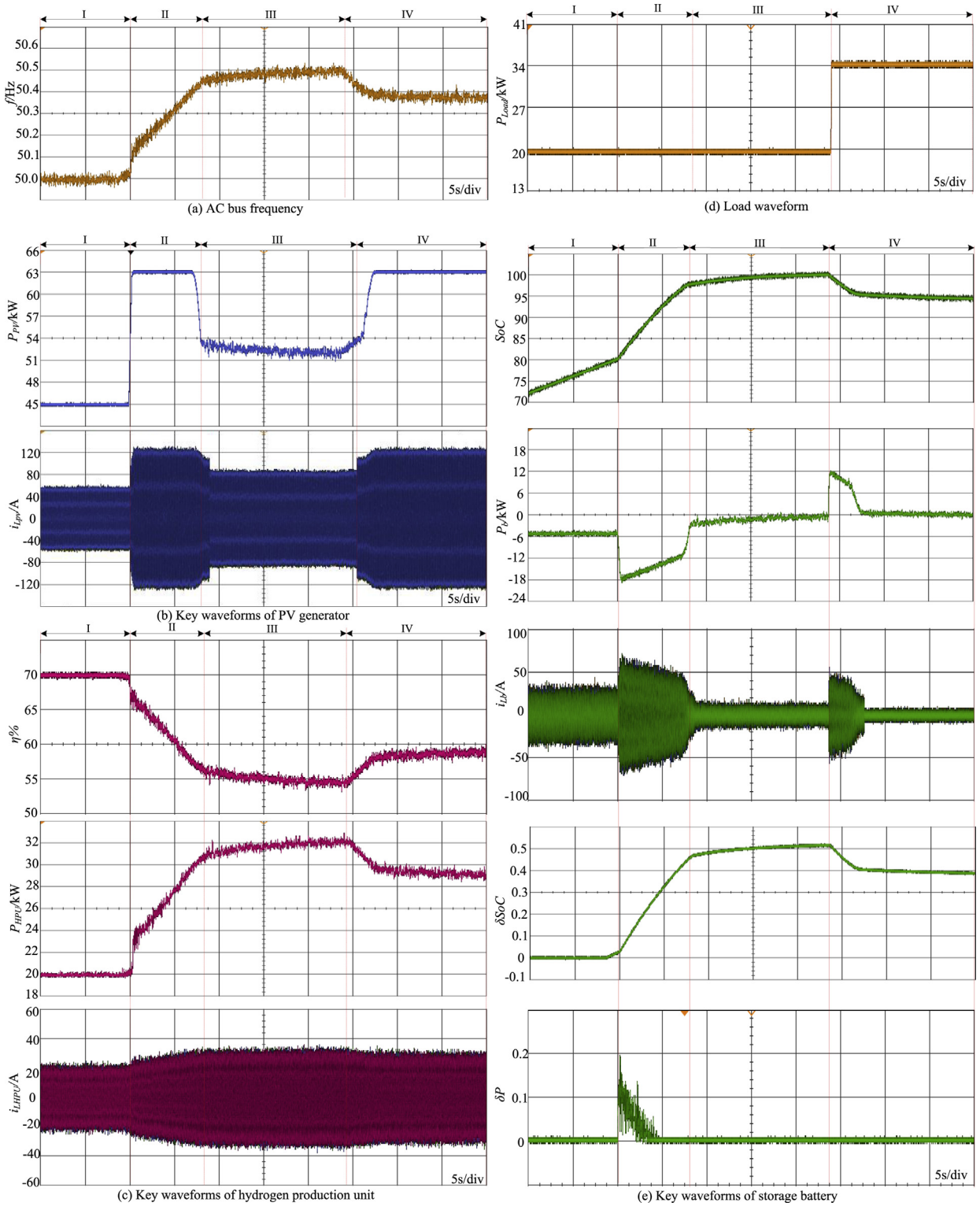

Fig. 10 – Control effectiveness in the sunny days.

off from the MEP to increase power absorption as much as possible. Finally, the PV output power is about 63 kW. HPU consumes about 32 kW. The local load consumes about 20 kW, and the surplus PV power will flow into the battery. The function result δSoC increases with the SoC. The function result δP is very large at the moment of the increase of PV power, but finally decreases to zero because the charging power is limited in the safe range.

During stage III, the bus frequency continues to increase because of the charging condition, and PV generator

Please cite this article as: Zhang Y, Wei W, Model construction and energy management system of lithium battery, PV generator, hydrogen production unit and fuel cell in islanded AC microgrid, International Journal of Hydrogen Energy, https://doi.org/10.1016/j.ijhydene.2020.04.155

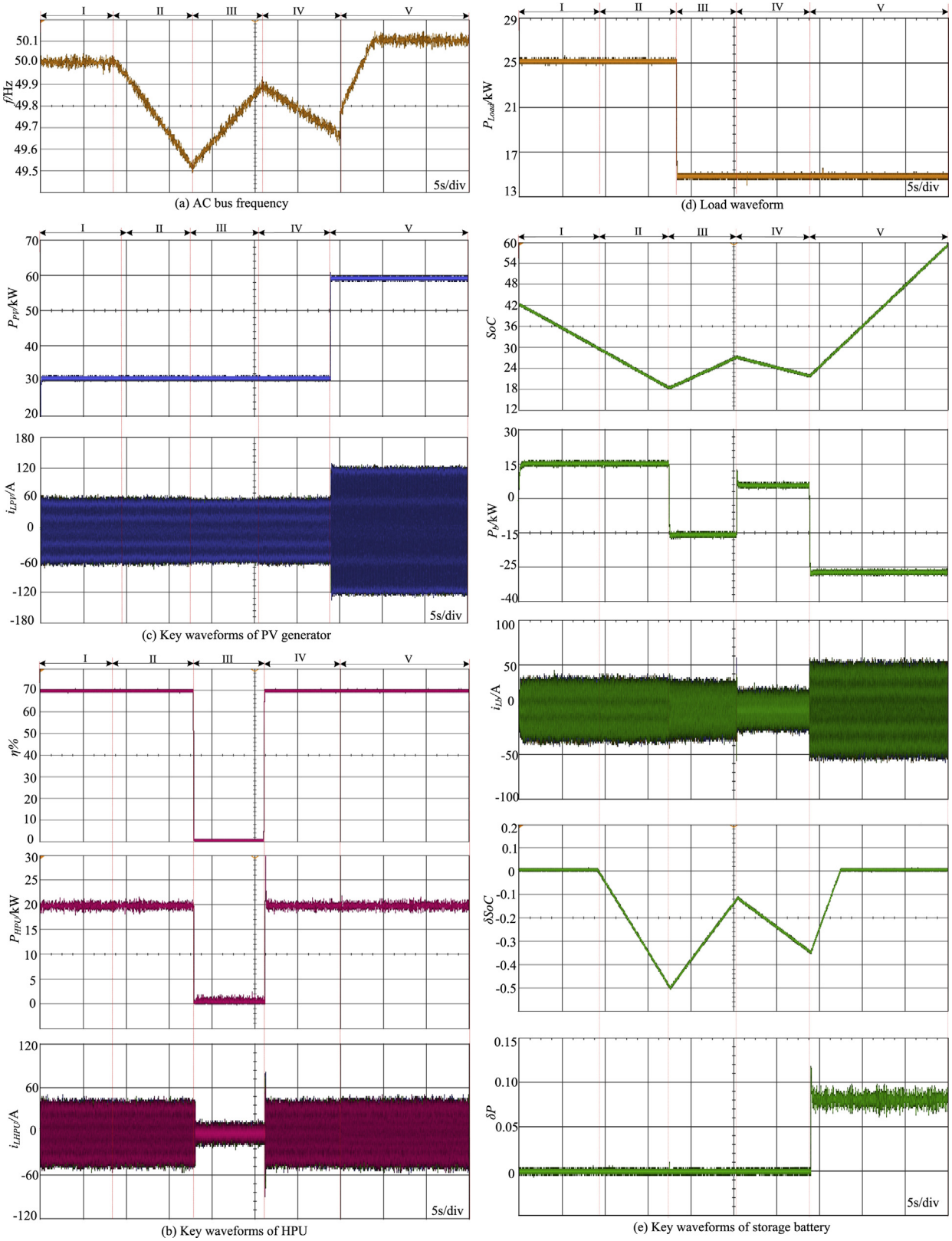

Fig. 11 – Control results in the cloudy or thunderstorm day.

Please cite this article as: Zhang Y, Wei W, Model construction and energy management system of lithium battery, PV generator, hydrogen production unit and fuel cell in islanded AC microgrid, International Journal of Hydrogen Energy, https://doi.org/10.1016/j.ijhydene.2020.04.155

adaptively reduces its power generation and works off from MPP mode. Finally, the PV output power is about 52 kW. HPU works at the allowable MPP mode and consumes about 32 kW. The local load consumes about 20 kW.

During stage IV, the load is increased to 34 kW, and the bus frequency is increased because of the discharging condition. Finally, the PV generation is about 63 kW, and HPU consumes 29 kW. Therefore, the lithium battery is floating charged. The function result δSoC decreases with the SoC, and the function result δP is zero finally.

Control results in the cloudy or thunderstorm day

The control results in the cloudy or thunderstorm day are shown in Fig. 11, in which the variables are the same as that in Fig. 10. The PV output power is limited because of the weak irradiance in the cloudy weather, and the battery discharges to help supply the local load and HPU. The waveforms are divided into five stages.

During stage I, the SoC is still larger than 30% in the discharging process, hence the bus frequency keeps at 50 Hz. PV generator operates at the MPP mode and the power generation is about 30 kW. The discharging power of the battery is about 15 kW, and the power consumption of the local load is about 25 kW. HPU works at the MEP mode and consumes 20 kW. Both the function results of Eqs (14) and (15) are zero as shown in Fig. 11(e).

During stage II, the SoC is continuous to decrease in the discharging condition and to cross over the setting value gradually. The AC bus frequency is reduced gradually because of the function result δSoC. But because f_{bus} is still larger than the setting value, HPU continuously works at MEP mode.

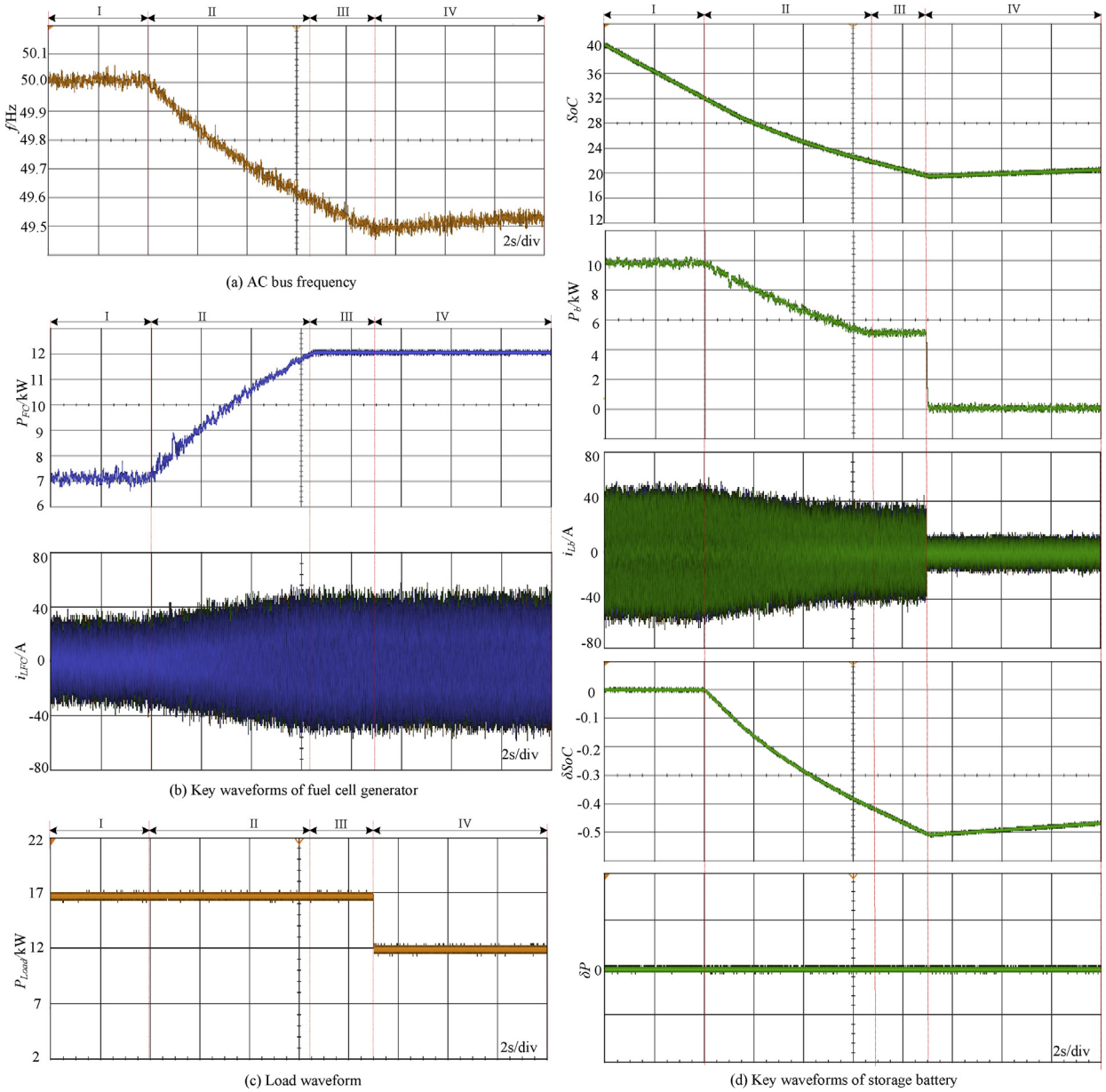

Fig. 12 – Control effectiveness at night.

Please cite this article as: Zhang Y, Wei W, Model construction and energy management system of lithium battery, PV generator, hydrogen production unit and fuel cell in islanded AC microgrid, International Journal of Hydrogen Energy, https://doi.org/10.1016/j.ijhydene.2020.04.155

During stage III, the AC bus frequency decreases to the setting value 49.5 Hz, hence HPU is cut out adaptively. In this situation, PV generator will supply the local load and charge the batteryat the same time. The PV output power is still 30 kW. Some unimportant load is cut out because the battery is configured with a small capacity, and the local load is 15 kW. The charging power is about 15 kW and the SoC will increase during this time. Because the function result δSoC increases gradually, the bus frequency increases accordingly. The function result δP is still zero.

During stage IV, HPU is put into operation again because the bus frequency increases to the setting value 49.9 Hz. In this situation, the PV output power is 30 kW. HPU works at MEP mode and consumes 20 kW. The local load remains at 15 kW. Therefore, the discharging power of the battery is about 5 kW. Then the bus frequency will decrease according to the function result δSoC.

During stage V, the strong irradiance is restored and the PV power generation is about 60 kW. Because the local load is 15 kW and HPU consumes 20 kW, there is extra 25 kW flowing into the battery. For one thing, the SoC increases rapidly and the function result δSoC will increase accordingly. For another thing, the charging power exceeds the setting value and the function result δP is produced thereby. But the SoC is relatively low, therefore a long period is necessary for the charging process. Then the working condition is transitioned to the first case.

Control results at night

The control results at night are shown in Fig. 12. Fig. 12(a) shows the waveform of the bus frequency f_{bus} Fig. 12(b) shows the waveforms of the fuel cell containing the power generation and three-phase inductive current. Fig. 12(c) shows the local load waveform. Fig. 12(d) shows the waveforms of the battery including the same variables as above-mentioned cases. The waveforms are divided into four stages.

During stage I, because the SoC of the battery is still relatively enough in the discharging process, f_{bus} continues to remain at 50 Hz. The fuel cell works at MEP mode to guarantee the high energy conversion efficiency, and the power generation is 7 kW. The battery discharging power is about 10 kW. The local load is about 17 kW. Because the SoC and the discharging power are in the safe range, the function results δSoC and δP are both zero. The duration of this process is determined by the capacity of the battery.

During stage II, because the SoC is decreased under the setting value, f_{bus} will decrease according to the function result δSoC. The fuel cell can perceive the variation of bus frequency and adjust its power generation adaptively. Finally, the fuel cell works at the allowable MPP mode and the power generation of the fuel cell is about 12 kW. The load power is about 17 kW. The function result δSoC will continue to decrease and the function result δP is still zero.

During stage III, because the discharging power of the battery is about 5 kW, the bus frequency decreases continuously. It should be pointed out that a large-capacity fuel cell can supply much more loads until the next day. But a small-capacity fuel cell is configured to rich the working conditions, and some unimportant loads needs to be cut out to stop the decrease of the bus frequency.

During stage IV, the SoC is still decreased in the discharging process and f_{bus} is decreased to the setting value 49.5 Hz. In this situation, some unimportant load is cut out, and the load power is about 12 kW, which is only supplied by the fuel cell finally. Meanwhile, the discharging power is about zero, and the SoC and the AC bus frequency keep unchanged until the next day. The function result δSoC keeps at -0.5 finally, and the function result δP is still remained at zero.

In summary, the designed energy management system of the islanded AC microgrid is verified in various situations. The two-stage energy conversion from electrical power to hydrogen gas and to electrical power is very low, therefore the fuel cell is not necessary to operate with the PV generator at the same time. A simple mutually exclusive working mode can be designed for the PV generator and the fuel cell by using a relay. When in the sunny day, the battery is getting charged first. Second, HPU can regulate its working point from MEP to MPP to absorb power as much as possible. Third, PV generator needs to limit its power generation and work off from MPP mode to RPP mode. When in the cloudy day, the battery discharges to help PV generator supply the local load and HPU first. Second, HPU needs to be cut out if the SoC is relatively low. Third, when the PV power generation is restored, HPU will be put into operation again. When at night, the fuel cell works at MEP mode to help the battery supply the local load first. Second, when the SoC is relatively low, the fuel cell needs to work from MEP mode to the allowable MPP mode to help supply the local load. The decentralized control strategy can save the communication lines and enhance the reliability of power supply.

Conclusion

The external electrical characteristics of the lithium battery, PV generator, HPU and fuel cell are analyzed according to their mathematic model, based on which an energy management system is designed for the islanded AC microgrid system.

As for the lithium battery, the functions with variables of SoC and instantaneous power are designed to guarantee that the remaining capacity of battery and the charging or discharging power are in the safe range. As for PV generator, the *P-f* droop control strategy is designed to make the PV generator work off from MPP mode to RPP mode seamlessly. As for HPU, the energy conversion efficiency is taken into consideration in the control strategy in order to make a trade off between the working efficiency and power consumption. As for the fuel cell, when the bus frequency locates at the rated value, the fuel cell will work at MEP mode with a small power generation. When the bus frequency decreases to deviate the rated value, the fuel cell will work from MEP mode to MPP mode to generate power as much as possible. Finally, the results based on RTLAB experimental platform are demonstrated to verify the effectiveness of the proposed control strategy.

In addition, the well-designed adaptive coordination control strategy is decentralized by using the common bus

Please cite this article as: Zhang Y, Wei W, Model construction and energy management system of lithium battery, PV generator, hydrogen production unit and fuel cell in islanded AC microgrid, International Journal of Hydrogen Energy, https://doi.org/10.1016/j.ijhydene.2020.04.155

frequency. Therefore, the communication lines are saved and the reliability of the AC microgrid system is enhanced.

Acknowledgements

This work was supported by the Key Research and Development Plan of Zhejiang Province (2019C01150) and National Key Research and Development Project (2017YFB0903300).

REFERENCES

[1] Rivarolo M, Rattazzi D, Magistri L. Best operative strategy for energy management of a cruise ship employing different distributed generation technologies. Int J Hydrogen Energy 2018;43(52):23500–10.
[2] Chen Hao, Yang Chen, Deng Kangjie, Zhou Nana, Wu Haochuang. Multi-objective optimization of the hybrid wind/solar/fuel cell distributed generation system using Hammersley Sequence Sampling. Int J Hydrogen Energy 2017;42(12):7836–46.
[3] Yamashita Daiji, Tsuno Katsuhiko, Koike Kayo, Fujii Katsushi, Wada Satoshi, Sugiyama Masakazu. Distributed control of a user-on-demand renewable-energy power-source system using battery and hydrogen hybrid energy-storage devices. Int J Hydrogen Energy 2019;44(50):27542–52.
[4] Rahbar K, Chai CC, Zhang R. Energy cooperation optimization in microgrids with renewable energy integration. IEEE Trans Smart Grid 2018;9(2):1482–93.
[5] Zhang Xiaoshun, Wang Dezhi, Tao Yu, Zhao Xu, Fan Zhun. Ensemble learning for optimal active power control of distributed energy resources and thermostatically controlled loads in an islanded microgrid. Int J Hydrogen Energy 2018;43(49):22474–86.
[6] Anastasiadis Anestis G, Konstantinopoulos Stavros A, Kondylis Georgios P, Vokas Georgios A, Papageorgas Panagiotis. Effect of fuel cell units in economic and environmental dispatch of a Microgrid with penetration of photovoltaic and micro turbine units. Int J Hydrogen Energy 2017;42(5):3479–86.
[7] Liang Zhanhao, Qin Yong, Wu Fengzhi, Ren Ziliang, Liu Yuzhi, Li Kun, Berti Stephen. Standalone condition diagnosing of fuel cell in microgrid composed of wind turbine/fuel cell/combined heat & power using Variational Mode Decomposition analysis model. Int J Hydrogen Energy 2018;43(39):18452–62.
[8] Aprilia E, Meng K, Al Hosani M, Zeineldin HH, Dong ZY. Unified power flow algorithm for standalone AC/DC hybrid microgrids. IEEE Trans Smart Grid 2019;10(1):639–49.
[9] Zhang Z, Miyajima R, Inada T, Miyagi D, Tsuda M. Novel energy management method for suppressing fuel cell degradation in hydrogen and electric hybrid energy storage systems compensating renewable energy fluctuations. Int J Hydrogen Energy 2018;43(14):6879–86.
[10] Fang Y, Jia K, Yang Z, Li Y, Bi T. Impact of inverter-interfaced renewable energy generators on distance protection and an improved scheme. IEEE Trans Ind Electron 2019;66(9):7078–88.
[11] Dui X, Zhu G, Yao L. Two-stage optimization of battery energy storage capacity to decrease wind power curtailment in grid-connected wind farms. IEEE Trans Power Syst 2018;33(3):3296–305.
[12] Jiang Yuewen, Deng Zhihong, Shi You. Size optimization and economic analysis of a coupled wind-hydrogen system with curtailment decisions. Int J Hydrogen Energy 2019;44(36):19658–66.
[13] Bhatt Mahesh Datt, Lee Jin Yong. High capacity conversion anodes in Li-ion batteries: a review. Int J Hydrogen Energy 2019;44(21):10852–905.
[14] Sánchez Mónica, Amores Ernesto, Abad David, Rodríguez Lourdes, Clemente-Jul Carmen. Aspen Plus model of an alkaline electrolysis system for hydrogen production. Int J Hydrogen Energy 2020;45(7):3916–29.
[15] El-Taweel NA, Khani H, Farag HEZ. Hydrogen storage optimal scheduling for fuel supply and capacity-based demand response program under dynamic hydrogen pricing. IEEE Trans Smart Grid 2019;10(4):4531–42.
[16] Garcia-Torres F, Bordons C. Optimal economical schedule of hydrogen-based microgrids with hybrid storage using model predictive control. IEEE Trans Ind Electron 2015;62(8):5195–207.
[17] Al Zohbi Gaydaa, Hendrick Patrick, Renier Christian, Bouillard Philippe. The contribution of wind-hydro pumped storage systems in meeting Lebanon's electricity demand. Int J Hydrogen Energy 2019;41(17):6996–7004.
[18] Wei F, Li Y, Sui Q, Lin X, Chen L, Chen Z, Li Z. A novel thermal energy storage system in smart building based on phase change material. IEEE Trans Smart Grid 2019;10(3):2846–57.
[19] Ghosh S, Kamalasadan S. An energy function-based optimal control strategy for output stabilization of integrated DFIG-flywheel energy storage system. IEEE Trans Smart Grid 2017;8(4):1922–31.
[20] Buckles W, Hassenzahl WV. Superconducting magnetic energy storage. IEEE Power Eng Rev 2000;20(5):16–20.
[21] Sun K, Zhang L, Xing Y, Guerrero JM. A distributed control strategy based on DC bus signaling for modular photovoltaic generation systems with battery energy storage. IEEE Trans Power Electron 2011;26(10):3032–45.
[22] Gu Y, Xiang X, Li W, He X. Mode-adaptive decentralized control for renewable dc microgrid with enhanced reliability and flexibility. IEEE Trans Power Electron 2014;29(9):5072–80.
[23] Lu X, Sun K, Guerrero JM, Vasquez JC, Huang L. Double-quadrant state-of-charge-based droop control method for distributed energy storage systems in autonomous dc microgrids. IEEE Trans Smart Grid 2015;6(1):147–57.
[24] Xia Y, Yu M, Yang P, Peng Y, Wei W. Generation-storage coordination for islanded dc microgrids dominated by PV generators. IEEE Trans Energy Convers 2019;34(1):130–8.
[25] Zhou T, Francois B, el Hadi Lebbal M, Lecoeuche S. Real-time emulation of a hydrogen-production process for assessment of an active wind-energy conversion system. IEEE Trans Ind Electron 2009;56(3):737–46.
[26] Bornapour Mosayeb, Hooshmand Rahmat-Allah, Khodabakhshian Amin, Parastegari Moein. Optimal stochastic coordinated scheduling of proton exchange membrane fuel cell-combined heat and power, wind and photovoltaic units in micro grids considering hydrogen storage. Appl Energy 2017;202:308–22.
[27] Nadaleti Willian Cézar, dos Santos Gabriel Borges, Lourenço Vitor Alves. The potential and economic viability of hydrogen production from the use of hydroelectric and wind farms surplus energy in Brazil: a national and pioneering analysis. Int J Hydrogen Energy 2020;45(3):1373–84.
[28] Hu Jiefeng, Shan Yinghao, Xu Yinliang, Josep M, Guerrero. A coordinated control of hybrid ac/dc microgrids with PV-wind-battery under variable generation and load conditions. Int J Electr Power Energy Syst 2019;104:583–92.
[29] Zhang Y, Wei W. Decentralised coordination control strategy of the PV generator, storage battery and hydrogen

Please cite this article as: Zhang Y, Wei W, Model construction and energy management system of lithium battery, PV generator, hydrogen production unit and fuel cell in islanded AC microgrid, International Journal of Hydrogen Energy, https://doi.org/10.1016/j.ijhydene.2020.04.155

production unit in islanded AC microgrid. IET Renew Power Gener 2020;14(6):1053–62.
[30] Liu S, Jiang J, Shi W, Ma Z, Wang LY, Guo H. Butler-volmer-equation-based electrical model for high-power lithium titanate batteries used in electric vehicles. IEEE Trans Ind Electron 2015;62(12):7557–68.
[31] Kim T, Qiao W. A hybrid battery model capable of capturing dynamic circuit characteristics and nonlinear capacity effects. IEEE Trans Energy Convers 2011;26(4):1172–80.
[32] Cai H, Xiang J, Wei W. Decentralized coordination control of multiple photovoltaic sources for DC bus voltage regulating and power sharing. IEEE Trans Ind Electron 2018;65(7):5601–10.
[33] Villalva MG, Gazoli JR, Filho ER. Comprehensive approach to modeling and simulation of photovoltaic arrays. IEEE Trans Power Electron 2009;24(5):1198–208.
[34] Zhang Y, Wei W. Decentralized coordination control of PV generators, storage battery, hydrogen production unit and fuel cell in islanded DC microgrid. Int J Hydrogen Energy 2020;45(15):8243–56.
[35] Ulleberg Øystein. Modeling of advanced alkaline electrolyzers: a system simulation approach. Int J Hydrogen Energy 2003;28(1):21–3.
[36] Wang MH, Huang M, Jiang W, Liou K. Maximum power point tracking control method for proton exchange membrane fuel cell. IET Renew Power Gener 2016;10(7):908–15.
[37] Chen X, Li W, Gong G, Wan Z, Tu Z. Parametric analysis and optimization of PEMFC system for maximum power and efficiency using MOEA/D. Applied Thermal Energy 2017;121:400–9.

Please cite this article as: Zhang Y, Wei W, Model construction and energy management system of lithium battery, PV generator, hydrogen production unit and fuel cell in islanded AC microgrid, International Journal of Hydrogen Energy, https://doi.org/10.1016/j.ijhydene.2020.04.155